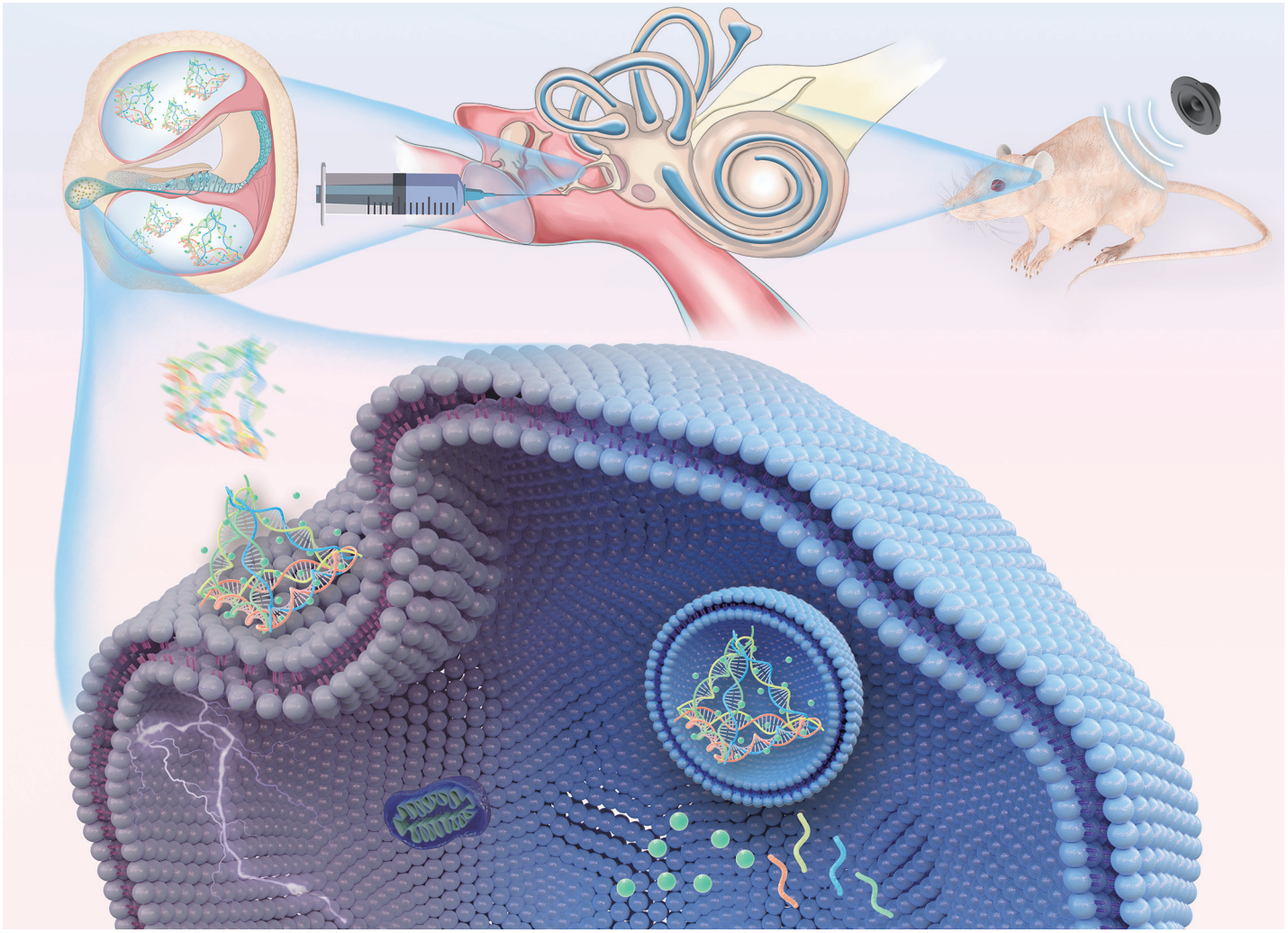

Showcasing research from Ear Institute, Shanghai Jiao Tong University School of Medicine, Shanghai 200011, People's Republic of China.

Epigallocatechin gallate-loaded tetrahedral DNA nanostructures as a novel inner ear drug delivery system

Epigallocatechin gallate (EGCG)-loaded tetrahedral DNA nanostructures (TDNs, EGCG@TDNs) have been successfully developed through non-covalent interactions, which effectively prevented cytotoxicity and apoptosis induced by lipid peroxidation *in vitro*. In addition, *in vivo* studies suggested that EGCG@TDNs significantly improved low-frequency hearing function in the noise-induced hearing loss model and the protective effect of EGCG@TDNs towards spiral ganglion neurons.

As featured in:

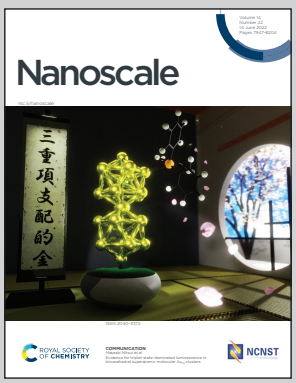

See Xueling Wang, Dehong Yu, Hao Wu *et al.*, *Nanoscale*, 2022, **14**, 8000.

ROYAL SOCIETY OF CHEMISTRY

rsc.li/nanoscale

Registered charity number: 207890

Nanoscale

PAPER

View Article Online
View Journal | View Issue

Cite this: *Nanoscale*, 2022, **14**, 8000

Epigallocatechin gallate-loaded tetrahedral DNA nanostructures as a novel inner ear drug delivery system†

Yuming Chen, ‡[a,b,c] Jiayi Gu,[a,b,c] Yan Liu,[d,e] Ke Xu,[a,b,c] Jie Song,[d,e] Xueling Wang,*[a,b,c] Dehong Yu*[a,b,c,f] and Hao Wu*[a,b,c]

The study of drug delivery systems to the inner ear is a crucial but challenging field. The sensory organ (in the inner ear) is protected by the petrous bone labyrinth and the membranous labyrinth, both of which need to be overcome during the drug delivery process. The requirements for such a delivery system include small size, appropriate flexibility and biodegradability. DNA nanostructures, biomaterials that can arrange multiple functional components with nanometer precision, exhibit characteristics that are compatible with the requirements for inner ear drug delivery. Herein, we report the development of a novel inner ear drug delivery system based on epigallocatechin gallate (EGCG)-loaded tetrahedral DNA nanostructures (TDNs, EGCG@TDNs). The TDNs self-assembled *via* base-pairing of four single-stranded DNA constructs and EGCG was loaded into the TDNs through non-covalent interactions. Cy5-labeled TDNs (Cy5-TDNs) were significantly internalized by the House Ear Institute-Organ of Corti 1 cell line, and this endocytosis was energy-, clathrin-, and micropinocytosis-dependent. Cy5-TDNs penetrated the round window membrane (RWM) rapidly *in vivo*. Local application of EGCG@TDNs onto the RWM of guinea pigs in a single dose continuously released EGCG over 4 hours. Drug concentrations in the perilymph were significantly elevated compared with the administration of free EGCG at the same dose. EGCG@TDNs were found to have favorable biocompatibility and strongly affected the RSL3-induced down-regulation of GPX4 and the generation of reactive oxygen species, on the basis of 2′,7′-dichlorodihydrofluorescein diacetate staining. JC-1 staining suggested that EGCG@TDNs successfully reversed the decrease in mitochondrial membrane potential induced by RSL-3 *in vitro* and rescued cells from apoptosis, as demonstrated by the analysis of Annexin V-FITC/PI staining. Further functional studies showed that a locally administered single-dose of EGCG@TDNs effectively preserved spiral ganglion cells in C57/BL6 mice after noise-induced hearing loss. Hearing loss at 5.6 and 8 kHz frequencies was significantly attenuated when compared with the control EGCG formulation. Histological analyses indicated that the administration of TDNs and EGCG@TDNs did not induce local inflammatory responses. These favorable histological and functional effects resulting from the delivery of EGCG by TDNs through a local intratympanic injection suggest potential for therapeutic benefit in clinical applications.

Received 2nd December 2021,
Accepted 20th April 2022

DOI: 10.1039/d1nr07921b

rsc.li/nanoscale

[a]*Department of Otolaryngology-Head and Neck Surgery, Shanghai Ninth People's Hospital, Shanghai Jiao Tong University School of Medicine, Shanghai 200011, People's Republic of China. E-mail: wuhao@shsmu.edu.cn, dehongyu@126.com, xuelingwang2013@163.com*
[b]*Ear Institute, Shanghai Jiao Tong University School of Medicine, Shanghai 200011, People's Republic of China*
[c]*Shanghai Key Laboratory of Translational Medicine on Ear and Nose Diseases (14DZ2260300), Shanghai 200011, People's Republic of China*
[d]*Institute of Nano Biomedicine and Engineering, Department of Instrument Science and Engineering, School of Electronic Information and Electrical Engineering, Shanghai Jiao Tong University, Shanghai 200240, People's Republic of China*
[e]*Institute of Cancer and Basic Medicine (ICBM), Chinese Academy of Sciences; The Cancer Hospital of the University of Chinese Academy of Sciences, Hangzhou, Zhejiang 310022, People's Republic of China*
[f]*Materdicine Lab, School of Life Sciences, Shanghai University, Shanghai, 200444, People's Republic of China*

†Electronic supplementary information (ESI) available. See DOI: **https://doi.org/10.1039/d1nr07921b**

‡First author.

Introduction

The delivery of sufficient drug concentrations to the sensory organ in the inner ear is a major unmet clinical need in the treatment of inner ear diseases such as idiopathic sudden sensorineural hearing loss, Ménière's disease and drug- or noise-induced hearing loss (NIHL).[1,2] The blood–brain barrier and blood-labyrinth barrier severely limit drug concentrations in the inner ear after intravenous or oral (systemic) administration.[3] The alternative to systemic administration is local drug delivery, which mainly includes intratympanic and intracochlear/intralabyrinthine delivery. Intracochlear drug delivery, in which the drug is directly released into the inner ear field, would give higher inner ear drug concentrations than either systemic or intratympanic delivery. However, intracochlear delivery requires surgery, which may cause secondary trauma in patients.[4] The most widely used method for drug delivery to the inner ear is intratympanic delivery, in which a drug solution is injected through the tympanic membrane into the middle ear.[5,6] Intratympanic delivery results in enhanced drug concentrations and reduces secondary trauma, but frequent administration is necessary to maintain drug concentrations in the inner ear.[4]

The rapid development of nano-based drug delivery systems in recent years may provide an alternative strategy to treat inner ear diseases.[2,7] Studies have shown significant protective effects of a dexamethasone sodium phosphate multivesicular liposome thermosensitive hydrogel and a novel outer hair cell-targeted/reactive oxygen species (ROS)-responsive nanoparticle berberine delivery system against noise-induced hearing impairment.[8,9] Liposomes modified with SS-31 have been investigated for improving the efficacy of minocycline against gentamicin-induced hearing loss and optimized phospholipid-based nanoparticles have been used to alleviate ototoxicity induced by kanamycin.[10,11] A variety of nanocarriers are currently being investigated for the treatment of inner ear diseases in clinical trials.[7] These delivery systems, however, still face challenges including limited round window membrane (RWM) and oval window membrane (OWM) penetration, long-term toxicity due to poor biocompatibility and low biodegradability.[1,4] Consequently, there is an imperative to develop novel carriers for inner ear drug delivery to meet the current clinical demand.

With great progress in the past four decades, various DNA nanostructures have been applied to different fields including single-molecule analysis, drug delivery, bioimaging, biosensing and DNA computing.[12–16] There has been a widespread study of DNA nanostructures for anti-cancer and anti-bacterial therapy because of their biocompatibility, biodegradability and versatility.[17,18] More importantly, based on the Watson–Crick base-pairing principle, homogeneous populations of DNA nanostructures can be assembled with precisely controlled size and shape, leading to their unique advantage of penetrating biological barriers such as skin.[19,20] The application of DNA nanostructures for the treatment of dermatological diseases has also attracted great attention in recent years.[19,20] Given the similarities of skin and RWM/OWM as biological barriers, we hypothesized that DNA nanostructures of a particular size and shape would be able to penetrate the RWM/OWM and serve as a new nanoplatform for the delivery of therapeutic agents into the inner ear.

Epigallocatechin gallate (EGCG), the most abundant catechin found in tea, exhibits various biological and pharmacological activities, including anti-inflammatory, antioxidant, antibacterial, and anti-tumor properties.[21–23] Studies have demonstrated that EGCG improves mitochondrial function, scavenges intracellular ROS and inhibits lipid peroxidation,[24–26] which make EGCG a candidate for the treatment of hearing loss treatment. Recent studies have demonstrated that EGCG can alleviate hearing loss induced by aminoglycoside antibiotics or cisplatin.[27,28] However, the low bioavailability, stability and poor solubility of EGCG greatly limit its use in clinical settings.[29,30] The encapsulation of EGCG in nano-sized vehicles has been considered as an approach to solve these problems.[21,22,30]

In this study, we aimed to evaluate the potential of DNA nanostructures with a specific shape and size for inner ear delivery. Furthermore, these DNA nanostructures could carry active drugs to alleviate sensorineural hearing loss as a new inner ear drug delivery system. In particular, tetrahedral DNA nanostructures (TDNs), which were most efficiently taken up by auditory hair cell lines of four synthesized DNA nanostructures, were selected as candidates for inner ear drug delivery. The cellular uptake and stability of TDNs were investigated *in vitro*. The feasibility of penetrating the RWM into the inner ear by TDNs was validated *in vivo*. As shown in Scheme 1, EGCG was loaded into TDNs *via* non-covalent interactions to construct a novel delivery system (EGCG@TDNs). The size, morphology, drug-loading profile and *in vivo* drug-release profile of EGCG@TDNs were investigated. The biological functions and mechanisms of EGCG@TDNs against RSL3-induced lipid peroxidation were demonstrated in an auditory cell line. Alleviation of noise-induced hearing loss by single dose intratympanic administration of EGCG@TDNs was investigated *in vivo*, which suggested great potential of these DNA nanostructures for inner ear drug delivery.

Results and discussion

Screening for optimal DNA nanostructures

The cellular uptake of a drug delivery system is crucial to obtain effective concentrations in cells. Since the size and shape have been identified as determinants for the cellular uptake of nanocarriers,[31] four different DNA nanostructures, including TDNs (7 nm side length), 6H × 73 nt (5.4 × 6 × 24 nm), 4 × 4 × 64 nt (8 × 8 × 22 nm) and 6 × 6 × 64 nt (12 × 12 × 22 nm), were designed and synthesized according to the previous literature for screening (Table 1, ESI,† Fig. 1A).[32,33] Meanwhile, as shown in Fig. 1A, in order to have the same molarity of Cy5 fluorophores, S1 and TDNs were tagged with one Cy5 fluorophore (Cy5-S1, Cy5-TDNs), 6H × 73 nt was tagged with three Cy5 fluorophores (Cy5-6H × 73 nt), and 4 × 4 × 64 nt and 6 × 6 × 64 nt were tagged with five Cy5 fluorophores (Cy5-4 × 4 × 64 nt, Cy5-6 × 6 × 64 nt). The successful

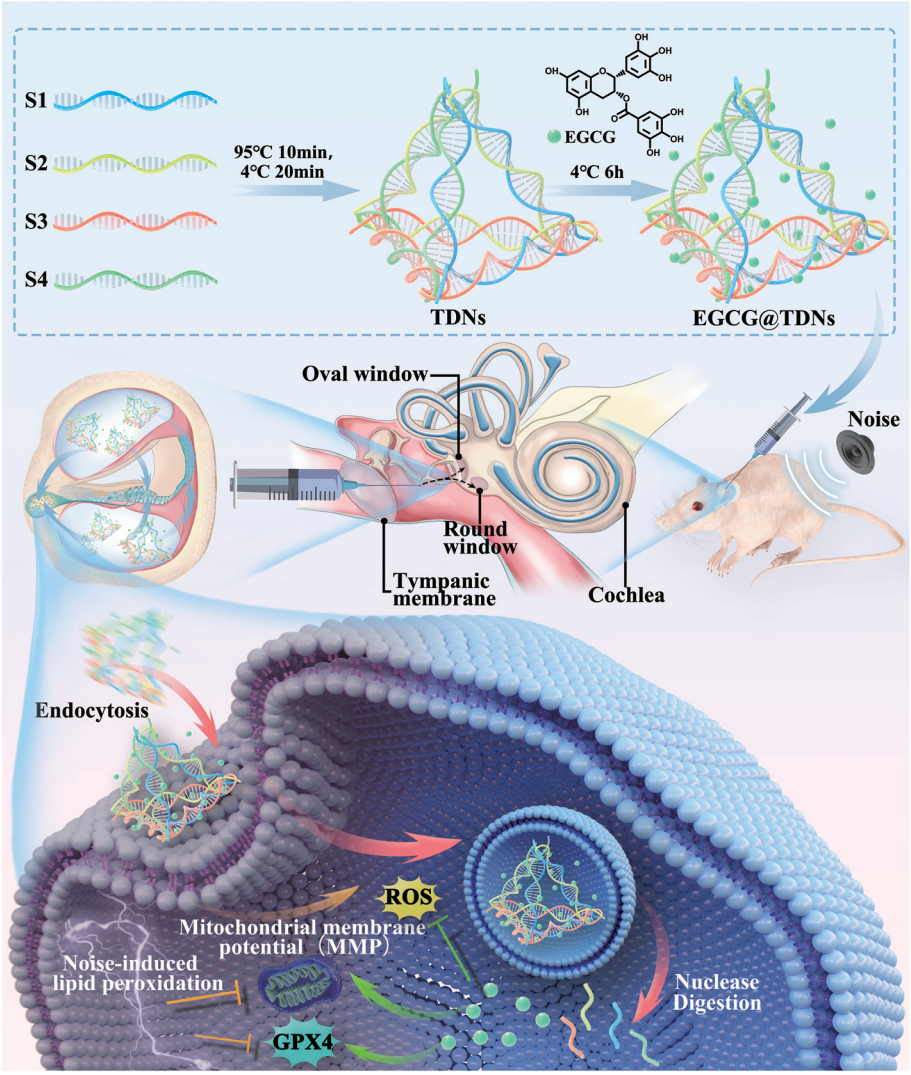

Scheme 1 Schematic showing the preparation of EGCG@TDNs and drug delivery to the inner ear for the treatment of noise-induced hearing loss.

synthesis of TDNs was verified by native polyacrylamide gel electrophoresis (PAGE), which showed that TDNs had the slowest migration rate compared with the four single strands, S1 + S2 and S1 + S2 + S3 (Fig. 1B), matching the 300 bp band from the DNA ladder. Atomic force microscopy (AFM) was used to examine TDNs and 6H × 73 nt, which showed that TDNs were tetrahedral and 6H × 73 nt was tubular in structure (Fig. 1C). Furthermore, transmission electron microscopy (TEM) showed that 4 × 4 × 64 nt and 6 × 6 × 64 nt had cubic structures (Fig. 1C). The House Ear Institute-Organ of Corti 1 (HEI-OC1) cell line, derived from the auditory organ of the transgenic mouse Immortomouse,[34] was used to evaluate the cellular uptake of the four DNA different nanostructures. Confocal images demonstrated markedly higher intracellular accumulation of TDNs than S1, 6H × 73 nt, 4 × 4 × 64 nt and 6 × 6 × 64 nt (Fig. 1D). Consequently, TDNs with a smaller size (7 nm), uniform shape (tetrahedral structure) and higher intracellular accumulation were selected for subsequent studies.

Cellular uptake profiles and mechanism of TDNs

The cellular uptake of Cy5-TDNs by HEI-OC1 cells was examined by confocal imaging and flow cytometry. Confocal images (Fig. S1A†) revealed the rapid uptake of TDNs by HEI-OC1 cells within 1 h. Moreover, the decreased intracellular fluorescence after 24 h incubation, according to flow cytometry statistical analysis, indicated the degradation of the TDNs (Fig. S1B†). The greater intracellular fluorescence intensity of Cy5-TDNs compared with Cy5-S1 after 24 h further suggested that the three-dimensional structure of TDNs is an important factor for cellular uptake. It was noted that the cellular uptake of TDNs after 6 h incubation was concentration-dependent (Fig. S1C and S1D†). Intracellular fluorescence intensity increased with increasing concentration of Cy5-TDNs but there was no signifi-

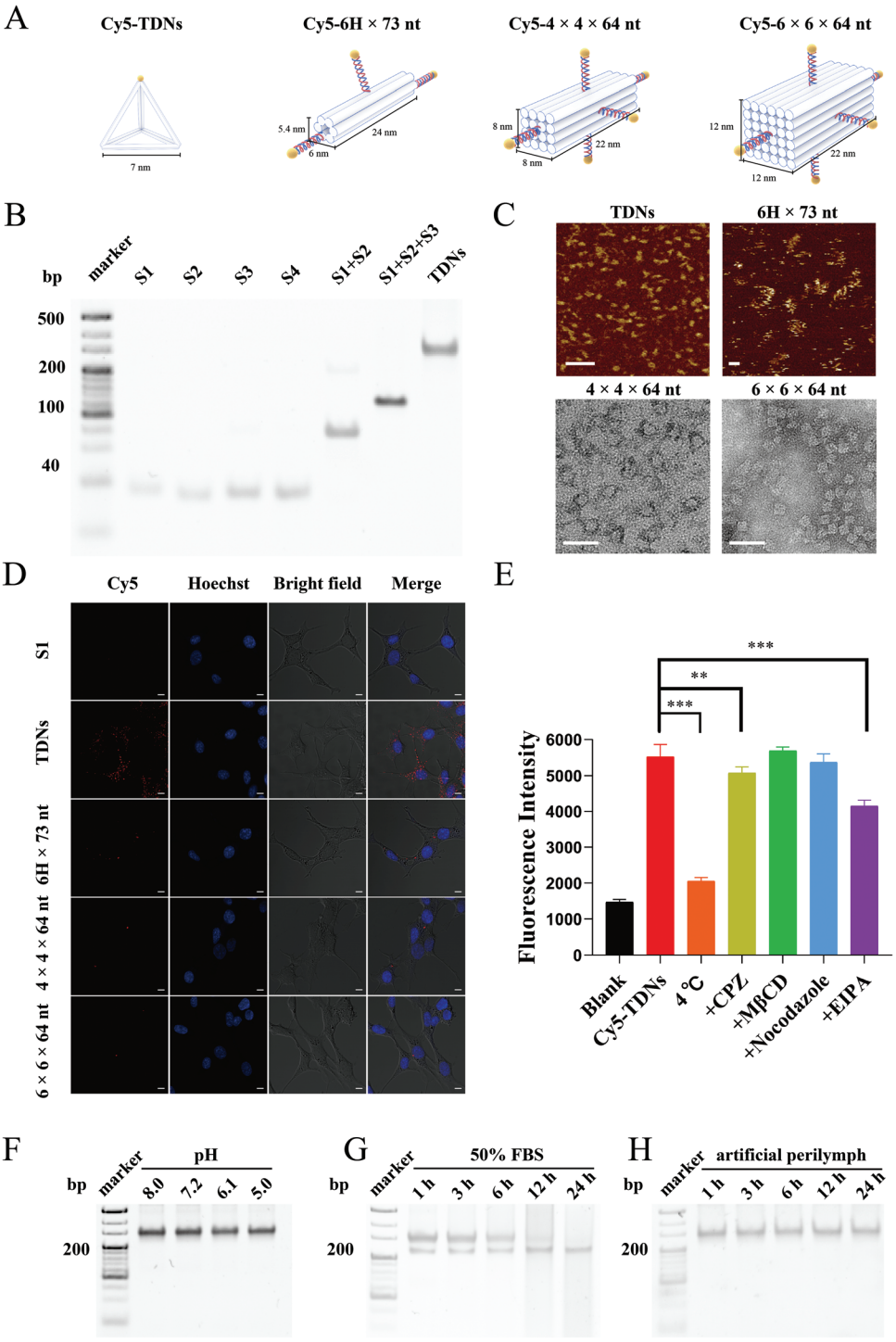

Fig. 1 Screening for optimal DNA nanostructures and characterization of TDNs. (A) Schematic illustration of Cy5-labeled TDNs, 6H × 73 nt, 4 × 4 × 64 nt and 6 × 6 × 64 nt nanostructures (Cy5-TDNs, Cy5-6H × 73 nt, Cy5-4 × 4 × 64 nt, Cy5-6 × 6 × 64 nt) (B) 8% Native polyacrylamide gel electrophoresis (PAGE) analysis of DNA single strands and TDNs. (C) Atomic force microscopy (AFM) images of TDNs and 6H × 73 nt and transmission electron microscopy (TEM) images of 4 × 4 × 64 nt and 6 × 6 × 64 nt nanostructures. AFM scale bar = 100 nm; TEM scale bar = 50 nm. (D) Confocal images of HEI-OC1 cells incubated with 150 nM Cy5-S1, 150 nM Cy5-TDNs, 50 nM Cy5-6H × 73 nt, 30 nM Cy5-4 × 4 × 64 nt and 30 nM Cy5-6 × 6 × 64 nt for 6 h. Scale bar = 10 μm. (E) Intracellular mean fluorescence intensity of HEI-OC1 cells incubated with 150 nM Cy5-TDNs at 4 °C for 6 h or pre-incubated with 20 μM inhibitors including CPZ, MβCD, EIPA and nocodazole for 1 h, followed by co-incubation with 150 nM Cy5-TDNs and 20 μM inhibitors for a further 6 h. Stability of TDNs in (F) different pH environments, (G) 50% FBS and (H) artificial perilymph for 24 h. Statistical significance: $^{**}P < 0.01$, $^{***}P < 0.001$.

cant difference between the 150 and 300 nM concentrations of Cy5-TDNs, which demonstrated the involvement of active transport in the cellular uptake of TDNs.

To explore the mechanism of Cy5-TDN internalization into HEI-OC1 cells, the effect of four different pathway inhibitors, including chlorpromazine (CPZ clathrin-dependent endocytosis), methyl-β cyclodextrin (MβCD, caveolin-dependent endocytosis), 5-(*N*-ethyl-*n*-isopropyl) amiloride (EIPA, pinocytosis), nocodazole (microtubules) and low temperature (4 °C) were studied. Intracellular fluorescence intensity was analyzed using a high content screening system. As shown in Fig. 1E, there was more than a half reduction (62.76 ± 1.84%, $p < 0.001$) in intracellular fluorescence intensity at 4 °C compared with 33 °C, indicating that the uptake of TDNs was energy-dependent. Interestingly, treatment of HEI-OC1 with MβCD or nocodazole did not markedly reduce the internalization of TDNs, with no significant decrease in fluorescence compared with TDNs at 33 °C. Thus, caveolin-dependent endocytosis and microtubules may not contribute to the cellular internalization of TDNs. In contrast, the fluorescence intensity significantly decreased in the presence of CPZ (8.09% ± 3.08%, $p < 0.01$) and EIPA (24.80% ± 2.88%, $p < 0.001$) compared with TDNs at 33 °C, suggesting that TDNs might be internalized by HEI-OC1 cells *via* multiple endocytic pathways, including micropinocytosis, and clathrin-mediated endocytosis. These results were different from previous reports that found the endocytosis of TDNs was caveolin-dependent in MCF-7, HeLa and COS-7 cell lines.[35,36] Since previous studies concluded that cellular receptors mediate the uptake of TDNs,[36] a possible explanation is that the expression levels of these receptors are significantly different in HEI-OC1 cells compared with those cells. The design of specific DNA nanostructures tailored to different organs, tissues and cells may therefore have potential for improving the efficacy of functional small molecules.

Stability studies

The stability of TDNs under various conditions was evaluated *in vitro* because of its importance in ensuring successful drug delivery. The pH and nuclease stabilities of TDNs were examined in serum-free medium at pH 5.0–8.0 or 50% fetal bovine serum (FBS) for 24 h. Native PAGE showed negligible changes in the TDN band after 24 h incubation at pH 5.0–8.0, suggesting no obvious disassembly of TDNs (Fig. 1F). This result demonstrated the strong stability of TDNs under different pH conditions. By contrast, TDNs were degraded gradually over time when incubated in 50% FBS, with a complete loss of the TDN band after 24 h incubation (Fig. 1G). This suggested the susceptibility of TDNs to the presence of nucleases, which was in good agreement with the previous literature.[37] Before absorption by different types of cells along the cochlear spiral, nanocarriers would remain in the perilymph of scala tympani and scala vestibuli after penetrating the RWM and OWM. Consequently, the stability of TDNs in the perilymph is critical for effective drug delivery. The stability of TDNs in artificial perilymph was therefore investigated in a mimicked physiological environment. The TDNs exhibited great stability in artificial perilymph, with no significant decrease in band intensity by native PAGE after 24 h incubation (Fig. 1H). This result suggested the minimal impact of the ion homeostasis microenvironment in the entire scala on the stability of TDNs, demonstrating another advantage of TDNs as nanocarriers for inner ear drug delivery.

Validating the feasibility of TDNs reaching the inner ear

Penetration of the biological barriers (RWM and OWM) between the middle and inner ear is a prerequisite for the application of TDNs for inner ear drug delivery. To determine whether TDNs could penetrate the RWM into the inner ear, gelfoam with Cy5-TDNs was placed on the round window niche using a retroauricular approach. RWM samples were scanned layer by layer using a confocal laser scanning microscope according to the reported method.[38] Confocal images (Fig. 2A and B) showed that TDNs rapidly penetrated the RWM, since a clear Cy5 fluorescent signal of TDNs was detected in the outer epithelium (OE) and connective tissue layers (CT) of the RWM 0.5 h after administration. Meanwhile, the fluorescence intensity decreased gradually from the OE towards the inner epithelium layer (IE), illustrating the penetration of the RWM by Cy5-TDNs. This process is more intuitively presented in 3D confocal images (Fig. 2C). Fig. 2D shows the mean fluorescence intensity in each layer of the RWM from the middle ear side to the inner ear side. The peak fluorescence intensity shifted from a depth of 7 nm at 0.5 h to 9 nm at 6 h, confirming the migration of Cy5-TDNs from the middle ear side to inner ear side of the RWM. Fluorescence was also measured in the cochleae of the Cy5-TDN-administered and contralateral sides using an *in vivo* imaging system (IVIS, Fig. 2E). The fluorescence intensity in the cochlea on the Cy5-TDN-administered side was markedly higher than that in the contralateral ear 0.5 h after administration. Finally, the perilymph was extracted from the cochleae and the fluorescence intensity was measured (Fig. 2F). As expected, the fluorescence intensity of the perilymph from the administered side was significantly higher than that on the contralateral side 0.5, 2 and 6 h after administration ($p < 0.001$). Overall, these results demonstrated the ability of TDNs to penetrate the RWM into the inner ear.

Characterization of EGCG@TDNs

To further explore the potential of TDNs for inner ear drug delivery, EGCG, a double-stranded DNA intercalator with antioxidant activity, was loaded into TDNs.[39,40] The morphologies and zeta potentials of TDNs and EGCG@TDNs were characterized. Uniform morphologies of TDNs and EGCG@TDNs, with minimal size difference, were observed by TEM imaging (Fig. 3A and S2†). The result demonstrated that EGCG loading did not significantly affect the original structure. As shown in Fig. 3B, the zeta potentials of TDNs, EGCG and EGCG@TDNs were −3.5, −9.7 and −4.3 mV, respectively. The successful intercalation of EGCG into TDNs was determined by UV-visible absorption measurements and fluorescence spectroscopic studies. The absorption spectra of TDNs and EGCG@TDNs

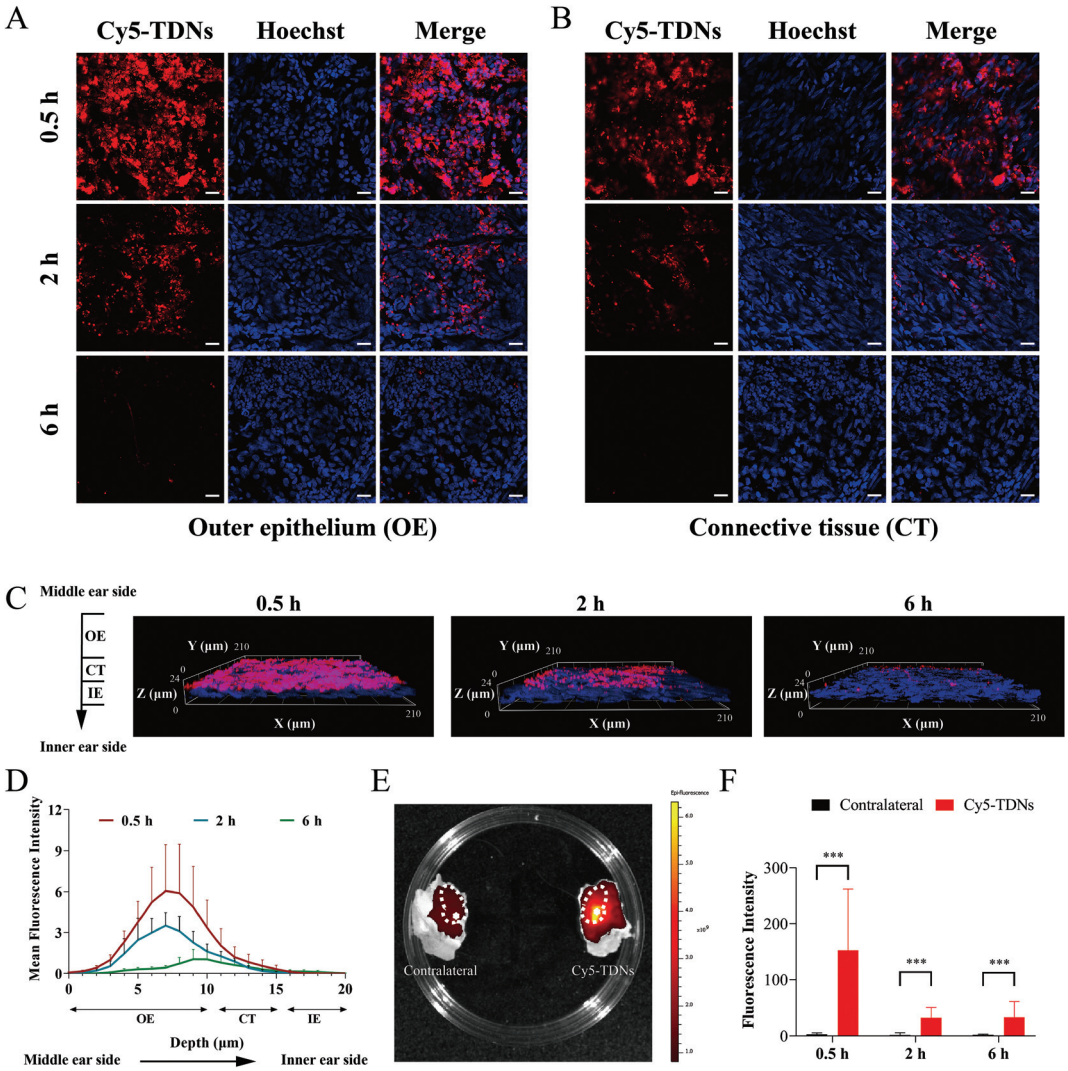

Fig. 2 Validating the feasibility of TDNs reaching the inner ear. Confocal images of (A) outer epithelium (OE) layer and (B) connective tissue (CT) layer of RWM treated with 2.5 μM Cy5-TDNs at different time points (0.5, 2 and 6 h). Scale bar = 20 μm. (C) 3D confocal images of RWM treated with 2.5 μM Cy5-TDNs at different time points (0.5, 2 and 6 h). (D) Mean fluorescence intensity of each layer of RWM from the middle ear side to the inner ear side in 1 μm steps treated with 2.5 μM Cy5-TDNs at different time points (0.5, 2 and 6 h). (E) IVIS images of cochleae treated with (Cy5-TDNs) or without (contralateral) 2.5 μM Cy5-TDNs for 0.5 h. The dotted circles represent the positions of the cochleae, and the asterisks represent the locations of the round window niches. (F) Fluorescence intensity of the perilymph extracted from cochleae treated with (Cy5-TDNs) or without (contralateral) 2.5 μM Cy5-TDNs at different timepoints (0.5, 2 and 6 h). Statistical significance: ***$P < 0.001$. Abbreviations: IE, inner epithelium.

after purification are shown in Fig. 3C. A notable decrease of the TDN absorption peak upon the addition of EGCG indicated the intercalation of EGCG into the dsDNA helix of TDNs. It is worth noting that similar results have been observed in the binding between flavonoids and quinones with dsDNA,[41–43] suggesting the possibility of loading compounds with similar structures into DNA nanostructures. The fluorescence spectroscopic studies were conducted based on previously reported methods.[32] The emission spectra of GelGreen bound to DNA in the absence or presence of EGCG are shown in Fig. 3D. The fluorescence intensity of EGCG@TDNs approached the baseline at a high concentration of EGCG, indicating that the intercalation of EGCG into TDNs was close to maximum loading. The fluorescence intensity of EGCG@TDNs decreased upon the addition of GelGreen dye, suggesting that the intercalation of EGCG into dsDNA competitively and partially inhibited the formation of the DNA-bound GelGreen fluorophore. The entrapment efficiency of EGCG was calculated according to the standard curve based on UV-visible absorption measurements at 272 nm (Fig. S3A†). The entrapment efficiencies were 55.5%, 56.8%, 45.2% and 27.3% under different TDN/EGCG molarity ratios (1 : 25, 1 : 50, 1 : 100, 1 : 200), respectively (Fig. S3B†). The optimal TDN/EGCG molarity ratio (1 : 100) was used in subsequent experiments considering that it provided almost saturated EGCG loading and high entrapment efficiency.

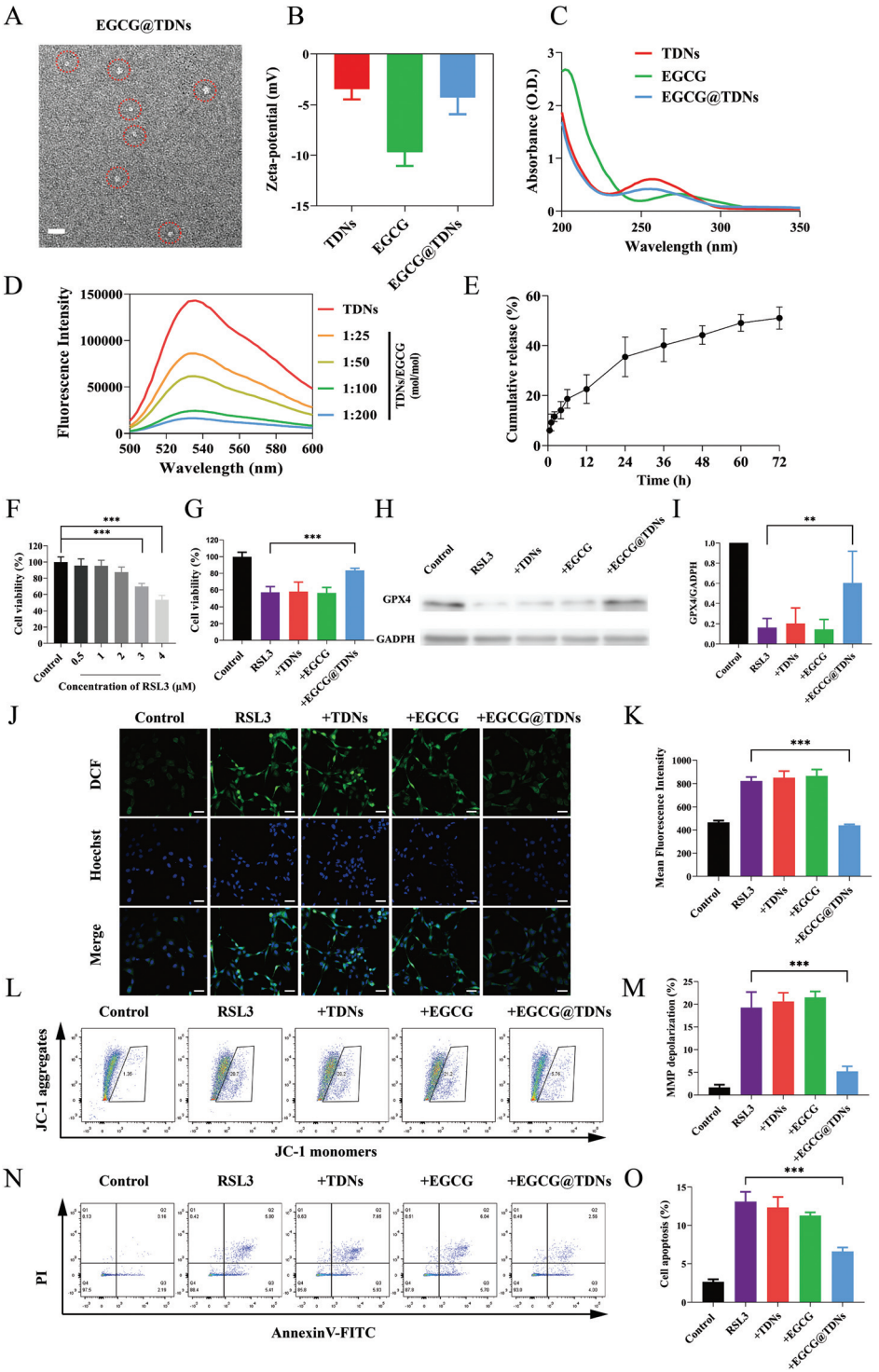

Fig. 3 Characterization of EGCG@TDNs and cellular experiments. (A) TEM image of EGCG@TDNs. The dotted circles represent the locations of EGCG@TDNs. Scale bar = 20 nm. (B) Zeta potentials of TDNs, EGCG and EGCG@TDNs. (C) The UV-visible absorption spectra of TDNs, EGCG and EGCG@TDNs. (D) The emission spectra of GelGreen bound to DNA in the absence or presence of EGCG under different TDN/EGCG molarity ratios (1 : 25, 1 : 50, 1 : 100, 1 : 200). (E) *In vitro* cumulative drug release profile of EGCG@TDNs at 37 °C in PBS solution (pH = 6.0). (F) Viability of HEI-OC1 cells incubated with a series of RSL3 concentrations (0.5, 1, 2, 3, 4 μM) for 24 h. (G) Viability of HEI-OC1 cells incubated with RSL3 (4 μM), RSL3 (4 μM) + TDNs/ + EGCG/ + EGCG@TDNs (1 μM) for 24 h. (H) Western blot analysis and (I) statistical analysis of GPX4 expression in HEI-OC1 cells after different treatments as mentioned above. (J) Confocal images and (K) high content screening statistical analysis of mean fluorescence intensity in HEI-OC1 cells performed by DCFH-DA staining after different treatments as mentioned above. Scale bar = 50 μm. (L) Flow cytometry and (M) statistical analysis of MMP depolarization percentages of HEI-OC1 cells performed by JC-1 staining after different treatments as mentioned above. (N) Flow cytometry and (O) statistical analysis of percentage apoptosis of HEI-OC1 cells performed by Annexin V-FITC/PI double staining after different treatments as mentioned above. Statistical significance: $^{**}P < 0.01$ and $^{***}P < 0.001$.

In vitro anti-lipid peroxidation and mechanism studies

Evidence indicates that lipid peroxidation and disruption of the ROS/antioxidant balance are both involved in NIHL.[44,45] The release of EGCG from EGCG@TDNs was evaluated in PBS solution (pH = 6.0), mimicking the acidic environment in inflamed cells, using a dialysis method.[46,47] Approximately 35% of the EGCG was rapidly released within 24 h, followed by sustained release over 72 h (Fig. 3E). To determine the optimal treatment concentration, HEI-OC1 cells were exposed to RSL3 (0, 0.5, 1, 2, 3 and 4 μM) for 24 h. Cell viability was 100% ± 6.449%, 95.526% ± 8.449%, 95.356% ± 6.978%, 87.542% ± 6.368%, 69.804% ± 3.855% and 53.482% ± 5.421% at each RSL3 concentration, respectively (Fig. 3F). The RSL3 (4 μM) 24 h treatment was selected for subsequent experiments since cell viability was closest to 50% under these conditions. The cytotoxicity of TDNs was examined at a series of concentrations (25, 50, 100, 250, 500 nM). No significant cytotoxicity was observed, indicating the good biocompatibility of TDNs as expected (Fig. S4A†). The cytotoxicity of free EGCG against HEI-OC1 cells was also determined. The results suggested that concentrations of EGCG below 5 μM had minimal impact on cell viability (Fig. S4B†).

Next, the cytoprotective effects of TDNs, EGCG and EGCG@TDNs against RSL3 damage were investigated. As shown in Fig. 3G, a significant increase of cell viability was only observed in the RSL3 + EGCG@TDN group, indicating that TDNs enhanced the bioavailability of EGCG. Previous studies have found that RSL3 induces intracellular accumulation of lipid peroxides by inactivating GPX4. Baicalein, a natural flavonoid, has been shown to have a protective effect against lipid peroxidation induced by RSL3, suggesting that EGCG may behave similarly.[48] We therefore examined the effect of EGCG@TDNs on the expression of GPX4 by western blot. The results (Fig. 3H and I) revealed that the expression of GPX4 in the RSL3 + EGCG@TDNs group was more than 3 times than that in the RSL3 group, suggesting that EGCG@TDNs partially restored GPX4 expression. Recent studies have indicated that the loss of GPX4 could increase cellular ROS production.[49,50] Hence, we determined intracellular ROS levels by 2′,7′-dichlorodihydrofluorescein diacetate staining. Confocal images (Fig. 3J) suggested that the intracellular ROS generation caused by RSL3 was remarkably suppressed by EGCG@TDNs. Statistical analysis of intracellular fluorescence intensity by high content screening showed that EGCG@TDNs reduced intracellular ROS to normal levels, with no significant difference between intracellular fluorescence in the control and RSL3 + EGCG@TDNs groups (Fig. 3K). This result further proved the antioxidant effect of EGCG@TDNs. Given that the mitochondrion is the main cellular organ that produces ROS, we next assessed mitochondrial function by analyzing the mitochondrial membrane potential (MMP) as measured by JC-1 staining. Flow cytometry and statistical analysis results showed that EGCG@TDNs significantly decreased the percentage of RSL-3-induced MMP depolarized cells from 19.30% to 5.24%, indicating that EGCG@TDNs improved mitochondrial function in RSL3-damaged cells (Fig. 3L and M). Considering that cell apoptosis could be triggered by the disruption of the oxidant/antioxidant balance, we finally investigated the anti-apoptotic properties of EGCG@TDNs by staining cells with Annexin V-FITC/PI. Unlike TDNs or EGCG, EGCG@TDNs significantly reduced the proportion of apoptotic cells (Fig. 3N and O). In particular, RSL3, RSL3 + TDNs and RSL3 + EGCG induced apoptosis in 13.11% ± 1.28%, 12.33% ± 1.40% and 11.28% ± 0.43% of cells, respectively, while RSL3 + EGCG@TDNs only induced apoptosis in 6.59% ± 0.53% of cells. Taken together, these results revealed the significant anti-lipid peroxidation activity of EGCG@TDNs as a consequence of improved mitochondrial function and antioxidant properties.

In vivo drug release profile and anti-noise-induced hearing loss (NIHL) studies

The increased lipid peroxidation and ROS could cause continued cochlear damage after the noise exposure.[45] We hypothesized that the high antioxidant activity of EGCG could alleviate hearing loss from noise trauma. As we mentioned earlier, sufficient drug concentration in the inner ear is crucial for treating NIHL. We first determined the *in vivo* release profiles of EGCG and EGCG@TDNs by measuring EGCG concentrations in the perilymph at different time points *via* LC–MS/MS analysis. The results, shown in Fig. 4A, indicated enhanced EGCG concentrations following a single intratympanic dose of EGCG@TDNs compared with free EGCG, suggesting the improvement of EGCG bioavailability and stability by TDNs. To study the antioxidant activity of EGCG@TDNs against NIHL, a mouse NIHL model was established by exposure to 106 dB sound pressure level noise with a bandpass of 8–16 kHz for 2 h. Auditory functions of the animals were evaluated on d0, d1, d7 and d14 (Fig. 4B). As shown in Fig. 4C, significant auditory brainstem response (ABR) threshold shifts were observed at all tested frequencies (4–32 kHz) on d1 and hearing function was partially restored at low frequencies (4–8 kHz) on d7. Furthermore, no significant differences were observed in mean ABR thresholds at the tested frequencies (4–32 kHz) between d7 and d14, suggesting the successful establishment of the NIHL model with a permanent threshold shift. The hearing function of NIHL mice after the intratympanic administration of TDNs, EGCG and EGCG@TDNs, was evaluated on d0, d1, and d14 (Fig. 4D–F). Compared with the contralateral ear, EGCG@TDN treatment produced a significant decline of mean ABR thresholds at 5.6 kHz ($p < 0.01$) and 8 kHz ($p < 0.001$) on d14, indicating a protective effect for low-frequency hearing. An obvious downward shift of mean ABR thresholds (no statistical difference) was also observed at rest frequencies (4 kHz ($p = 0.0664$), 11.3 kHz ($p = 0.0664$), 16 kHz ($p > 0.9999$), 22.3 kHz ($p = 0.1478$) and 32 kHz ($p = 0.2145$)). However, neither TDNs nor free EGCG improved auditory function in the treated ear compared to the contralateral ear, which indicated that EGCG@TDNs enhanced the bioavailability of EGCG. These results indicated that EGCG@TDNs gave better protection of low-frequency hearing in the NIHL model. This

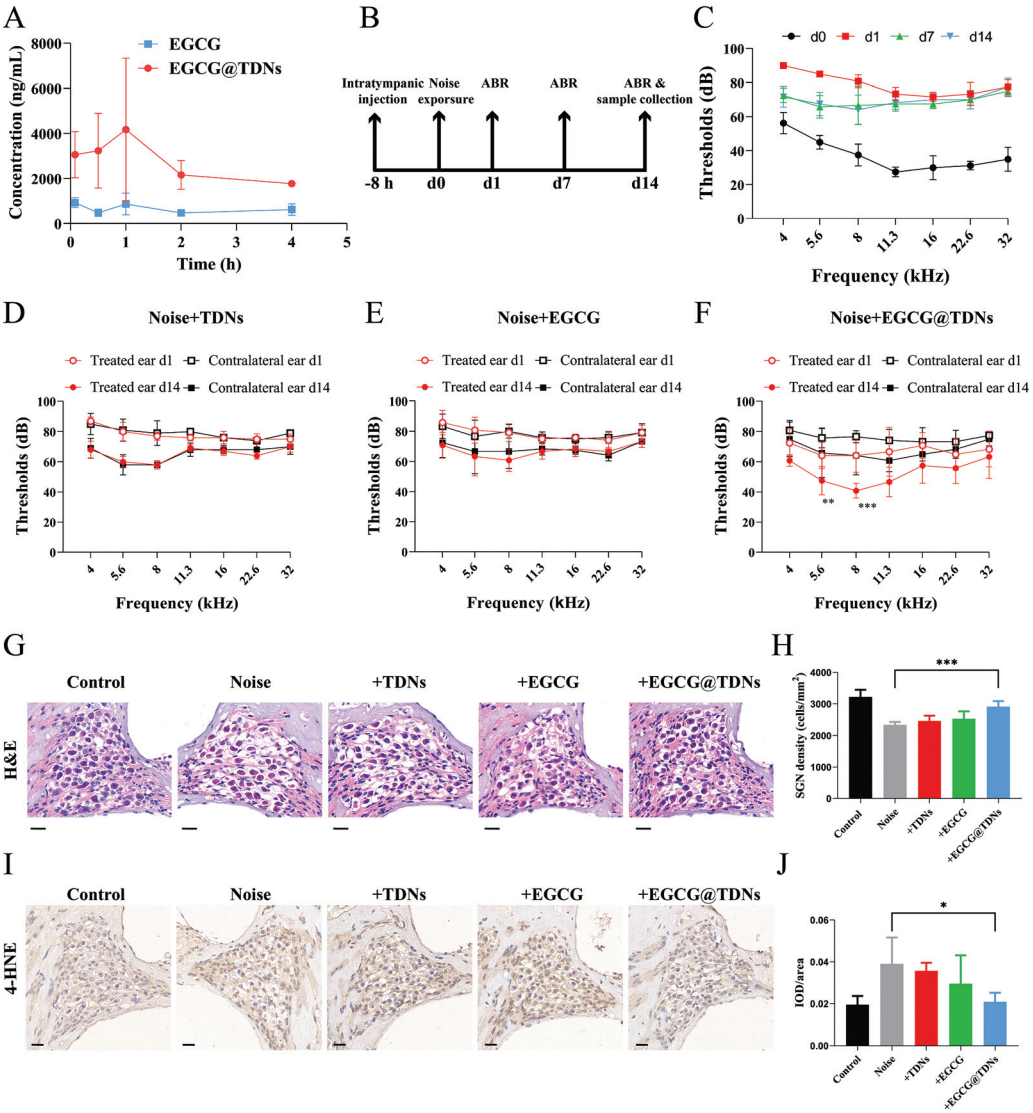

Fig. 4 *In vivo* anti-noise-induced hearing loss (NIHL) studies. (A) EGCG concentrations in the perilymph during 4 h after the intratympanic injection of 100 μM EGCG and EGCG@TDNs (n = 6). (B) Diagrammatic showing time course after the intratympanic injection of TDNs, EGCG and EGCG@TDNs. (C) Auditory function of mice subjected to noise exposure (106 dB, 8–16 kHz, 2 h) on d0, d1, d7 and d14 (n = 5). ABR recordings of (D) noise + TDNs (n = 5), (E) noise + EGCG (n = 6) and (F) noise + EGCG@TDNs (n = 6) on d0, d1, d14. (G) H&E staining images of SGNs and (H) SGN densities in different groups. Scale bar = 20 μm (n = 5). (I) 4-HNE expression in SGNs performed by DAB staining and (J) integrated optical density (IOD)/area in different groups (n = 5). Scale bar = 20 μm. *P < 0.05, **P < 0.01 and ***P < 0.001.

could be because noise-induced damage is relatively less in the low-frequency range than that in the high-frequency area,[51] or because noise-induced vibration of the RWM and OWM may promote the distribution of EGCG@TDNs towards the apical turn (low frequency area).[52]

No obvious loss of outer hair cells was observed in our NIHL model (106 dB, 8–16 kHz, 2 h). However, hematoxylin and eosin (H&E) staining demonstrated that acute noise exposure resulted in the loss of spiral ganglion neurons (SGNs, Fig. 4G), which was consistent with previous studies.[53,54] Intriguingly, histology and the corresponding quantitative data revealed that SGN density was significantly enhanced in the low-frequency area (4–8 kHz) after EGCG@TDNs treatment, indicating the prevention of SGN apoptosis by EGCG@TDNs (Fig. 4H). To evaluate lipid peroxidation levels in the cochleae, 4-hydroxynonenal, a specific biomarker of lipid peroxidation, was stained using a 3,3′-diaminobenzidine (DAB) kit. The DAB staining images (Fig. 4I) indicated the increased accumulation of lipid peroxides in the cochlea after noise exposure. Integrated optical density (IOD) values were collected and used to calculate the average density (IOD/area). The results of statistical analysis showed that treatment with EGCG@TDNs effectively reduced lipid peroxidation levels in SGNs (Fig. 4J), in accordance with our *in vitro* results. These results demonstrated that EGCG@TDNs prevent low-frequency hearing loss in the NIHL

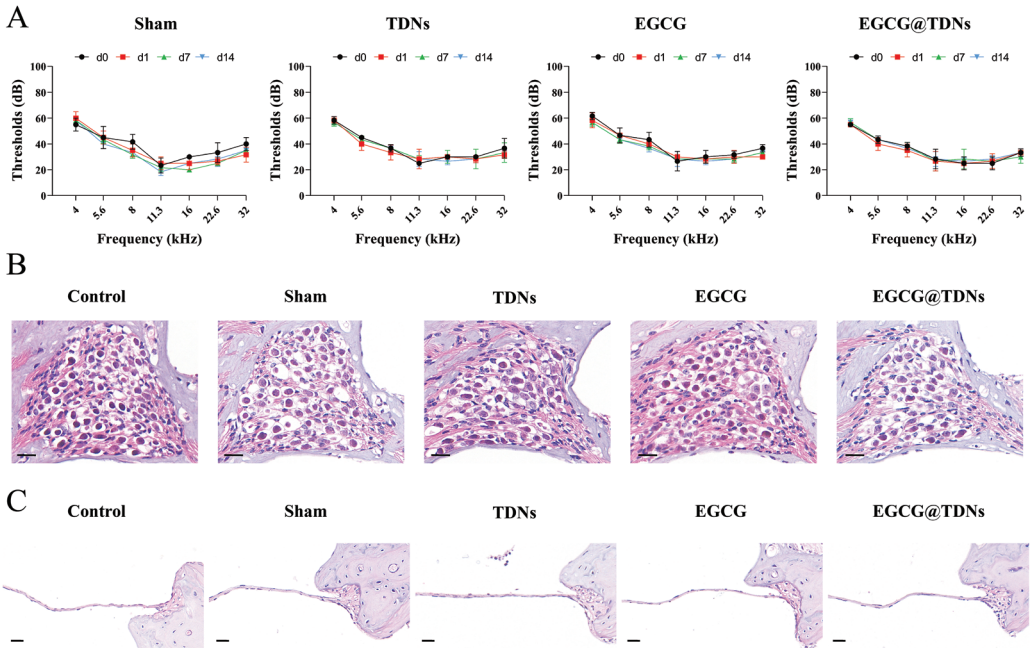

Fig. 5 Safety evaluation. (A) ABR recordings following different treatments on d0, d1, d7 and d14 (n = 3). Images of (B) SGNs and (C) oval membrane morphology performed by H&E staining 14 days after different treatments. Scale bar = 20 μm.

model by reducing lipid peroxide accumulation in the cochlea and preserving SGNs.

Safety evaluation

The safety of the novel EGCG@TDNs drug delivery system was evaluated by ABR measurements and histological studies. As shown in Fig. 5A, the mean ABR thresholds of sham, TDN, EGCG and EGCG@TDN treated animals were not significantly different compared with the control on d14, indicating the negligible impact of animal surgery or the above agents on hearing function. Furthermore, no obvious infection or effusion was observed in the middle ear cavity of any animals before they were sacrificed. The H&E staining of a cochlear section also demonstrated that during the surgical procedure, TDNs, EGCG and EGCG@TDNs did not induce obvious morphological changes of SGNs or the OWM (Fig. 5B and C). All of these findings demonstrate the excellent biocompatibility of EGCG@TDNs, which is crucial for clinical application.

Conclusion

In summary, we have demonstrated that TDNs readily penetrate the RWM into the inner ear. The EGCG@TDN formulation was successfully synthesized *via* non-covalent interactions and effectively prevented cytotoxicity and apoptosis induced by lipid peroxidation *in vitro*. Experimental data suggested that EGCG@TDNs reversed the decrease in GPX4 expression, improved mitochondrial function and reduced levels of intracellular ROS induced by RSL3. In addition, ABR recordings suggested that EGCG@TDNs significantly improved low-frequency hearing function in the NIHL model. The protective effect of EGCG@TDNs towards SGNs and the down-regulation of lipid peroxidation accumulation were demonstrated by histological assessment. This is, to the best of our knowledge, the first study demonstrating the potential of DNA nanostructures for drug delivery in inner ear therapy. We believe that our results provide new insights into the design and development of novel carriers for inner ear drug delivery.

Conflicts of interest

There are no conflicts to declare.

Acknowledgements

The present study was supported by the Natural Science Foundation of Shanghai (No. 19ZR1429400 and No. 21ZR1437600), the National Natural Science Foundation of China (No. 81970874), the State Key Program of National Natural Science Foundation of China (No. 81330023), and the Shanghai Key Laboratory of Translational Medicine on Ear and Nose Diseases (No. 14DZ2260300), and the Innovative Research Team of High-level Local universities in Shanghai. We thank International Science Editing (**https://www.internationalscienceediting.com**) for editing this manuscript and Shanghai Institute of Precision Medicine for providing instruments including flow cytometry and high content screening system.

References

1 Y. Ma, A. K. Wise, R. K. Shepherd and R. T. Richardson, *Pharmacol. Ther.*, 2019, **200**, 190–209.
2 L. Li, T. Chao, J. Brant, B. O'Malley Jr., A. Tsourkas and D. Li, *Adv. Drug Delivery Rev.*, 2017, **108**, 2–12.
3 Z. Huang, Q. Xie, S. Li, Y. Zhou, Z. He, K. Lin, M. Yang, P. Song and X. Chen, *Front. Cell Dev. Biol.*, 2021, **9**, 750185.
4 S. Nyberg, N. J. Abbott, X. Shi, P. S. Steyger and A. Dabdoub, *Sci. Transl. Med.*, 2019, **11**, aao0935.
5 T. Nakashima, I. Pyykko, M. A. Arroll, M. L. Casselbrant, C. A. Foster, N. F. Manzoor, C. A. Megerian, S. Naganawa and Y. H. Young, *Nat. Rev. Dis. Primers*, 2016, **2**, 16028.
6 M. Patel, K. Agarwal, Q. Arshad, M. Hariri, P. Rea, B. M. Seemungal, J. F. Golding, J. P. Harcourt and A. M. Bronstein, *Lancet*, 2016, **388**, 2753–2762.
7 R. Mittal, S. A. Pena, A. Zhu, N. Eshraghi, A. Fesharaki, E. J. Horesh, J. Mittal and A. A. Eshraghi, *Artif. Cells, Nanomed., Biotechnol.*, 2019, **47**, 1312–1320.
8 Z. Zhao, Z. Han, K. Naveena, G. Lei, S. Qiu, X. Li, T. Li, X. Shi, W. Zhuang, Y. Li, Y. Qiao and H. Liu, *ACS Appl. Mater. Interfaces*, 2021, **13**, 7102–7114.
9 Y. Li, R. Zhang, X. Li, W. Li, Y. Lu and C. Dai, *Exp. Cell Res.*, 2020, **387**, 111755.
10 S. Hou, Y. Yang, S. Zhou, X. Kuang, Y. Yang, H. Gao, Z. Wang and H. Liu, *Biomater. Sci.*, 2018, **6**, 1627–1635.
11 K. J. Yang, J. Son, S. Y. Jung, G. Yi, J. Yoo, D. K. Kim and H. Koo, *Biomaterials*, 2018, **171**, 133–143.
12 K. Cervantes-Salguero, M. Freeley, J. L. Chávez and M. Palma, *J. Mater. Chem. B*, 2020, **8**, 6352–6356.
13 T. Wu, J. Liu, M. Liu, S. Liu, S. Zhao, R. Tian, D. Wei, Y. Liu, Y. Zhao, H. Xiao and B. Ding, *Angew. Chem., Int. Ed.*, 2019, **58**, 14224–14228.
14 S. M. Douglas, J. J. Chou and W. M. Shih, *Proc. Natl. Acad. Sci. U. S. A.*, 2007, **104**, 6644–6648.
15 P. S. Kwon, S. Ren, S. J. Kwon, M. E. Kizer, L. Kuo, M. Xie, D. Zhu, F. Zhou, F. Zhang, D. Kim, K. Fraser, L. D. Kramer, N. C. Seeman, J. S. Dordick, R. J. Linhardt, J. Chao and X. Wang, *Nat. Chem.*, 2020, **12**, 26–35.
16 J. Chao, J. Wang, F. Wang, X. Ouyang, E. Kopperger, H. Liu, Q. Li, J. Shi, L. Wang, J. Hu, L. Wang, W. Huang, F. C. Simmel and C. Fan, *Nat. Mater.*, 2019, **18**, 273–279.
17 A. Lacroix and H. F. Sleiman, *ACS Nano*, 2021, **15**, 3631–3645.
18 Y. Yuan, Z. Gu, C. Yao, D. Luo and D. Yang, *Small*, 2019, **15**, 1900172.
19 K. Jiang, Y. Chen, D. Zhao, J. Cheng, F. Mo, B. Ji, C. Gao, C. Zhang and J. Song, *Nanoscale*, 2020, **12**, 18682–18691.
20 C. Wiraja, Y. Zhu, D. C. S. Lio, D. C. Yeo, M. Xie, W. Fang, Q. Li, M. Zheng, M. Van Steensel, L. Wang, C. Fan and C. Xu, *Nat. Commun.*, 2019, **10**, 1147.
21 V. Aggarwal, H. S. Tuli, M. Tania, S. Srivastava, E. E. Ritzer, A. Pandey, D. Aggarwal, T. S. Barwal, A. Jain, G. Kaur, K. Sak, M. Varol and A. Bishayee, *Semin. Cancer Biol.*, 2020, **80**, 256–275.
22 A. Rashidinejad, S. Boostani, A. Babazadeh, A. Rehman, A. Rezaei, S. Akbari-Alavijeh, R. Shaddel and S. M. Jafari, *Food Res. Int.*, 2021, **142**, 110186.
23 J. Duan, Z. Chen, X. Liang, Y. Chen, H. Li, X. Tian, M. Zhang, X. Wang, H. Sun, D. Kong, Y. Li and J. Yang, *Biomaterials*, 2020, **255**, 120199.
24 I. Scala, D. Valenti, V. Scotto D'Aniello, M. Marino, M. P. Riccio, C. Bravaccio, R. A. Vacca and P. Strisciuglio, *Antioxidants (Basel)*, 2021, **10**, 469.
25 S. Lee, J. Lee, H. Byun, S. J. Kim, J. Joo, H. H. Park and H. Shin, *Acta Biomater.*, 2021, **124**, 166–178.
26 M. Bruckner, S. Westphal, W. Domschke, T. Kucharzik and A. Lugering, *J. Crohn's Colitis*, 2012, **6**, 226–235.
27 V. Borse, R. F. H. Al Aameri, K. Sheehan, S. Sheth, T. Kaur, D. Mukherjea, S. Tupal, M. Lowy, S. Ghosh, A. Dhukhwa, P. Bhatta, L. P. Rybak and V. Ramkumar, *Cell Death Dis.*, 2017, **8**, 2921.
28 L. T. Gu, J. Yang, S. Z. Su, W. W. Liu, Z. G. Shi and Q. R. Wang, *Neurochem. Res.*, 2015, **40**, 1211–1219.
29 N. Tyagi, R. De, J. Begun and A. Popat, *Int. J. Pharm.*, 2017, **518**, 220–227.
30 K. Li, C. Teng and Q. Min, *Front. Chem.*, 2020, **8**, 573297.
31 C. Kinnear, T. L. Moore, L. Rodriguez-Lorenzo, B. Rothen-Rutishauser and A. Petri-Fink, *Chem. Rev.*, 2017, **117**, 11476–11521.
32 T. Zhang, T. Tian, R. Zhou, S. Li, W. Ma, Y. Zhang, N. Liu, S. Shi, Q. Li, X. Xie, Y. Ge, M. Liu, Q. Zhang, S. Lin, X. Cai and Y. Lin, *Nat. Protoc.*, 2020, **15**, 2728–2757.
33 Y. F. Zhong, J. Cheng, Y. Liu, T. Luo, Y. Wang, K. Jiang, F. Mo and J. Song, *Small*, 2020, **16**, 2003646.
34 G. Kalinec, P. Thein, C. Park and F. Kalinec, *Hear. Res.*, 2016, **335**, 105–117.
35 K. R. Kim, D. R. Kim, T. Lee, J. Y. Yhee, B. S. Kim, I. C. Kwon and D. R. Ahn, *Chem. Commun.*, 2013, **49**, 2010–2012.
36 L. Liang, J. Li, Q. Li, Q. Huang, J. Shi, H. Yan and C. Fan, *Angew. Chem., Int. Ed.*, 2014, **53**, 7745–7750.
37 A. R. Chandrasekaran, *Nat. Rev. Chem.*, 2021, **5**, 225–239.
38 L. Zhang, Y. Xu, W. Cao, S. Xie, L. Wen and G. Chen, *Int. J. Nanomed.*, 2018, **13**, 479–492.
39 X. Zheng, A. Chen, T. Hoshi, J. Anzai and G. Li, *Anal. Bioanal. Chem.*, 2006, **386**, 1913–1919.
40 R. Galindo-Murillo and T. E. Cheatham 3rd, *J. Biomol. Struct. Dyn.*, 2018, **36**, 3311–3323.
41 H. Zhou, Z. Sun, T. Hoshi, Y. Kashiwagi, J. Anzai and G. Li, *Biophys. Chem.*, 2005, **114**, 21–26.
42 Z. Sun, Z. Ma, W. Zhang, X. Wang, C. Fan and G. Li, *Anal. Bioanal. Chem.*, 2004, **379**, 283–286.
43 Y. Sun, S. Bi, D. Song, C. Qiao, D. Mu and H. Zhang, *Sens. Actuators, B*, 2008, **129**, 799–810.
44 I. Varela-Nieto, S. Murillo-Cuesta, M. Calvino, R. Cediel and L. Lassaletta, *Expert Opin. Drug Discovery*, 2020, **15**, 1457–1471.
45 D. Henderson, E. C. Bielefeld, K. C. Harris and B. H. Hu, *Ear Hear.*, 2006, **27**, 1–19.

46 S. Martin-Saldana, R. Palao-Suay, M. R. Aguilar, L. Garcia-Fernandez, H. Arevalo, A. Trinidad, R. Ramirez-Camacho and J. San Roman, *J. Controlled Release*, 2018, **270**, 53–64.
47 F. Zhang, G. Zhu, O. Jacobson, Y. Liu, K. Chen, G. Yu, Q. Ni, J. Fan, Z. Yang, F. Xu, X. Fu, Z. Wang, Y. Ma, G. Niu, X. Zhao and X. Chen, *ACS Nano*, 2017, **11**, 8838–8848.
48 M. Yang, X. Li, H. Li, X. Zhang, X. Liu and Y. Song, *Biochem. Biophys. Res. Commun.*, 2021, **561**, 65–72.
49 X. Jiang, B. R. Stockwell and M. Conrad, *Nat. Rev. Mol. Cell Biol.*, 2021, **22**, 266–282.
50 X. Chen, R. Kang, G. Kroemer and D. Tang, *Nat. Rev. Clin Oncol.*, 2021, **18**, 280–296.
51 F. Wu, H. Xiong and S. Sha, *Redox Biol.*, 2020, **29**, 101406.
52 S. M. Flaherty, I. J. Russell and A. N. Lukashkin, *Drug Delivery*, 2021, **28**, 1312–1320.
53 S. Khoshsirat, H. A. Abbaszadeh, A. A. Peyvandi, F. Heidari, M. Peyvandi, L. Simani and S. Niknazar, *J. Chem. Neuroanat.*, 2021, **114**, 101956.
54 S. M. Vlajkovic, K. Ambepitiya, M. Barclay, D. Boison, G. D. Housley and P. R. Thorne, *Hear. Res.*, 2017, **345**, 43–51.